Article

JOURNAL OF COMPOSITE MATERIALS

Journal of Composite Materials
2017, Vol. 51(5) 721–730

DOI: 10.1177/0021998316649252
journals.sagepub.com/home/jcm
SAGE

Shock attenuation mechanisms of magnetorheological elastomers absorbers: A theoretical analysis

Dingxin Leng[1,2], Xiaojie Wang[3,4], Lingyu Sun[1] and Faramarz Gordaninejad[3]

Abstract

To predict the dynamic response of shock absorbers based on magnetorheological elastomers and investigate the contributions of various possible energy dissipation mechanisms, a modified four-parameter model of magnetorheological elastomers was proposed, which includes the viscoelastic characteristics of rubber matrix, the variable stiffness and damping property, and the interfacial bond conditions of magnetorheological elastomers under the applied magnetic field. The constitutive equations of magnetorheological elastomers were derived and all parameters were identified based on a published literature. It is theoretically demonstrated that the maximum response force under an impulse input could be attenuated approximately 30% when the magnetic field with 0.57 T is applied. Using the proposed theoretical model, it is shown that the energy dissipation mechanisms mainly come from the interfacial friction between particles and matrix, and the increment on stiffness and dynamic viscosity of the rubber matrix provides reverse contributions to the shock mitigation, while the interfacial bond stiffness has little influence on the response force amplitude. Hence, when magnetorheological elastomers are utilized in shock absorbers, it is suggested to take advantage of the interfacial friction energy.

Keywords

Magnetorheological elastomers, four-parameter model, shock absorber, dynamic response

Introduction

At various shock or impact situations such as earthquakes, bomb explosions, and automobile collisions, an effective way for structure protection is to apply shock absorbers. Most conventional shock absorbers are passive and effective only on special conditions, which are unsatisfied for all payloads with various impacting mass, velocities, amplitudes, and directions. Therefore, adaptive shock-mitigation devices are especially necessary to active or semiactive controls. Magnetorheological (MR) materials are known to have variable stiffness and damping properties under changeable applied magnetic field and hence are promotional candidates for shockproof.[1] Several years ago, magnetorheological fluid (MRF) dampers have been experimentally demonstrated effectively in attenuating impact peak and lowering vibration level.[2–4] However, the settlement and instability of pending particles and leakage of fluid in MRF limit its application at diverse directions.

As the solid counterpart of MRFs, magnetorheological elastomers (MREs)[5] fabricated typically by dispersing iron particles into elastomer under magnetic fields, have neither deposition, sealing problems nor environmental contamination, and are easy to be manufactured. MREs have been verified to be effective in controllable-stiffness components,[6] and most related researches mainly focus on the material preparation,

[1]School of Transportation Science and Engineering, Beihang University, Beijing, China
[2]Department of Mechanical and Electrical Engineering, Ocean University of China, Qingdao, China
[3]Mechanical Engineering Department, University of Nevada, Reno, USA
[4]Institute of Advanced Manufacturing Technology, Hefei Institute of Physical Science, Chinese Academy of Sciences, Changzhou, China

Corresponding author:
Lingyu Sun, School of Transportation Science and Engineering, Beihang University, Beijing 100191, China.
Email: lysun@buaa.edu.cn

mechanical tests, physical modeling, and vibration application.[7–12] Recently, the possibility of applying their field-response damping properties in shock mitigation[7,13] has also been investigated. Fu et al.[14] studied experimentally a MRE buffer under impact loading and found that the peak acceleration response can be reduced largely due to the magnetic field effect. Additionally, our previous work[15] has also investigated numerically the failure modes of macroparticle-reinforced MREs under impact loading, which showed that the failure degree is largely related to the magnetic flux density. However, the influence of various factors (such as stiffness, damping, or field-induced stress) in MREs on its dynamic response (such as peak force and energy dissipation) is seldom studied and some energy dissipation mechanisms are still unknown, which are important to the design of MREs-based shock absorber.

In this paper, we will investigate the impact response of MRE shock absorber theoretically. The viscoelastic model of MREs without magnetic field will be introduced, and then, the multiparameter viscoelastic–plastic models with magnetic field will be provided to describe the rheological characteristics of MREs in off/on-states, and the constitutive equation of MREs will be derived. Using them, the theoretical model of MREs-based shock absorber under impulse loading will be established and solved numerically. Additionally, all parameters will be normalized and identified based on a published literature, which will be used in the subsequent numerical investigation. Finally, the dynamic impact responses of MRE-based shock absorber will be analyzed, and the effect of magnetic field and the contribution of individual parameters on the energy dissipation will be investigated at time domain.

Methodologies

Typically, the models of MREs can be divided into two types: micromodel and macromodel.[16]

Using the micromodel, the effects of particle shape, particle-chain orientation, and stress distributions in MREs are studied by continuum mechanics,[17,18] and the MR effect and shear modulus are investigated by the interaction theory of dipole magnetic particles.[19] In the micromodel, the local stress and magnetization field can be clearly analyzed. However, this method has to adopt some simplified assumptions on the local coupled mechanical and magnetic distribution.[20]

Using the macromodel, the relationship between force–displacement and stress–strain for different loading modes of MREs can be studied by applying the combination of viscoelastic and nonlinear elements.[21–23] The field-dependent modulus could be obtained by simulation using variable-stiffness spring. However, there is a weakness on describing the interfacial interaction between the particles and matrix. To overcome this issue, Chen and Jerrams[24] proposed a model including the field-induced stress, in which a variable-stiffness spring was used to simulate the field-dependent properties, and the damping viscosity was set to a constant. Nevertheless, some studies stated that the damping properties of MREs also changed with the variable magnetic field.[9] In our following modeling, all the viscoelasticity, field-induced modulus and damping viscosity, and interfacial bond stress of MREs will be considered.

Theoretical modeling of MREs

Viscoelastic properties of off-state MREs. The matrix of MREs is rubber, which is a typical viscoelastic material. Therefore, when no magnetic field is applied, the mechanical properties of elastomer composites could be simulated approximately by a standard linear solid model.[24] As shown in Figure 1, G_a and G_b represent the shear stiffness of rubber matrix and the interface phase, respectively, and η expresses the dynamic viscosity of the dashpot element.

Therefore

$$\gamma_1 = \frac{\tau_1}{G_a} + \int_0^t \frac{\tau_1}{\eta}\,\mathrm{d}t \tag{1}$$

$$\gamma_2 = \frac{\tau_2}{G_b} \tag{2}$$

$$\gamma = \gamma_1 = \gamma_2 \tag{3}$$

$$\tau = \tau_1 + \tau_2 \tag{4}$$

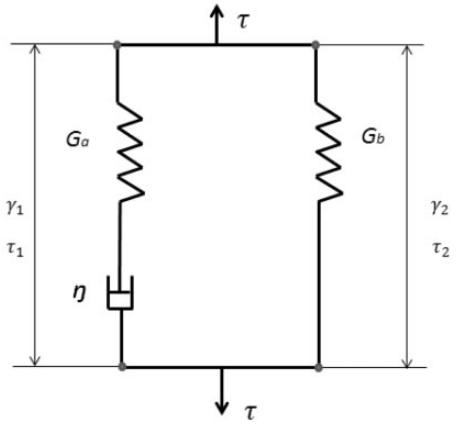

Figure 1. Three-parameter model for off-state MREs.

where τ and γ are the total shear stress and shear strain, respectively. And γ_n and τ_n ($n=1$ and 2) are the corresponding stress and strain of each branch, respectively. The constitutive equation can be expressed as

$$\tau + \kappa_r \cdot \dot{\tau} = G_b \cdot (\gamma + \kappa_t \cdot \dot{\gamma}) \tag{5}$$

where κ_r and κ_t are viscoelastic parameters, which can be calculated by

$$\kappa_r = {}^{\eta}/_{G_a} \tag{6}$$

$$\kappa_t = \frac{\eta \cdot (G_a + G_b)}{G_a \cdot G_b} \tag{7}$$

Magnetic field-induced mechanical properties of MREs. In on-state, the embedded ferromagnetic particles are magnetized. The magnetic forces among internal particles affect the field-induced modulus and damping properties, which are simulated by the variable stiffness and damping, as shown in the left branch in Figure 2. In addition, the interfacial bond condition between embedded particles and matrix leads to the field-dependent stress, which is simulated by a friction component and a spring element, as shown in the right branch in Figure 2.

In the left branch, the resultant deformation of spring and dashpot elements is constantly proportional to the external loading. In the right branch, the mechanical behaviors are divided into two stages. At the first stage, the load is so small that the friction slider is nearly fixed, and the length of the springs is only determined by the loading amplitude. Hence, MRE behaves as a linear viscoelastic material. With increasing loads, the interfacial stress may achieve the critical value, $\sigma_y(B)$, the interfacial bond strength of MREs.

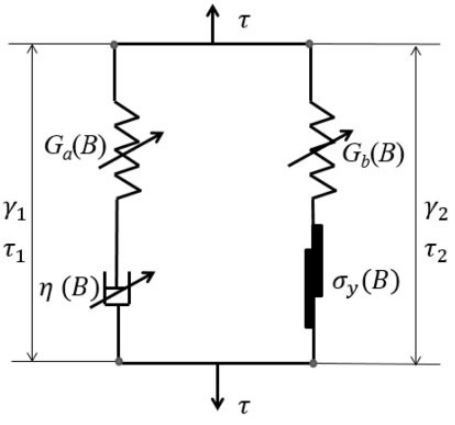

Figure 2. Four-parameter model for on-state MRE.

Then, the second stage begins: the friction slider starts to slip and the spring with stiffness G_b retains a constant length. The piecewise constitutive model is established as follows, and the reverse loading is similar.

In the first stage, the stress and strain relationship can be expressed as

$$\tau + \kappa_r(B) \cdot \dot{\tau} = G_b(B) \cdot (\gamma + \kappa_t(B) \cdot \dot{\gamma}) \tag{8}$$

where

$$\kappa_r(B) = {}^{\eta(B)}/_{G_a(B)} \tag{9}$$

$$\kappa_t(B) = \frac{\eta(B) \cdot (G_a(B) + G_b(B))}{G_a(B) \cdot G_b(B)} \tag{10}$$

In the second stage, the relationships between stress and strain can be expressed as

$$\gamma_1 = \frac{\tau_1}{G_a(B)} + \int_o^t \frac{\tau_1}{\eta(B)} \mathrm{d}t \tag{11}$$

$$\tau_2 = \sigma_y(B) \cdot sgn\{\dot{\gamma}(t)\} \tag{12}$$

Therefore

$$\tau + \kappa_r(B) \cdot \dot{\tau} = \eta(B) \cdot \dot{\gamma} + \sigma_y(B) \cdot sgn\{\dot{\gamma}(t)\} \tag{13}$$

In order to eliminate the numerical singularities, $S = \tanh(\frac{\dot{\gamma}}{a})$, is introduced, which replaces the *sgn* function in equation (13), thus

$$\tau + \kappa_r(H) \cdot \dot{\tau} = \eta(H) \cdot \dot{\gamma} + \sigma_y(H) \cdot S\{\dot{\gamma}(t)\} \tag{14}$$

where a is the control parameter for S, as 0.0001 mm/s.[25]

The interfacial bond strength of MREs, $\sigma_y(B)$, can be obtained as the maximum value of the field-induced stress, $\sigma_f(B)$, which is calculated by taking the derivative of the diploe energy density, U, with respect to the strain, $\bar{\gamma}$

$$\sigma_f(B) = \frac{\partial U}{\partial \bar{\gamma}} \tag{15}$$

Figure 3 shows the interface slider diagram of two adjacent magnetic particles in a chain along with the direction of applied magnetic field.

In Figure 3, r_0 is the distance between two adjacent particles, related to the volume fraction of magnetic particles, φ. $|M|$ is the dipole moment

$$|M| = J_p \cdot V_i \tag{16}$$

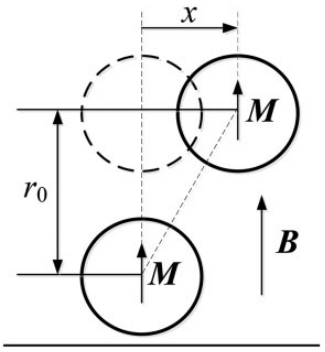

Figure 3. The slider diagram of magnetic particles at microscale.[27]

where J_p is the diploe moment magnitude per unit particle volume, and V_i is the unit particle volume

$$J_p = \mu_0 \cdot M_p \tag{17}$$

where M_p is the magnetization, which can be expressed as

$$M_p = \frac{(\mu_p - 1) \cdot M_s \cdot B}{\mu_p \cdot M_s + (\mu_p - 1) \cdot B} \tag{18}$$

where μ_p is the relative permeability of magnetic particles, and M_s is the saturated magnetization of ferromagnetic materials.

The strain $\bar{\gamma}$ can be calculated as

$$\bar{\gamma} = \frac{x}{r_0} \tag{19}$$

The magnetic energy density can be expressed as[26]

$$U = \frac{3 \cdot \varphi \cdot (\bar{\gamma}^2 - 2) \cdot |M|^2}{2 \cdot \pi^2 \cdot \mu_1 \cdot \mu_0 \cdot d^3 \cdot r_0^2 \cdot (1 + \bar{\gamma}^2)^{5/2}} \tag{20}$$

where μ_1 is the relative permeability of elastomers. μ_0 is the vacuum permeability, $4\pi \times 10^{-7}$ N/A^2. And d is the particle diameter.

Combining equations (15) to (19), the interfacial bond strength can be expressed as

$$\sigma_f(B) = \frac{\varphi \cdot \mu_0 \cdot (\mu_p - 1)^2 \cdot M_s^2 \cdot B^2 \cdot \bar{\gamma} \cdot (4 - \bar{\gamma}^2)}{\mu_p^2 \cdot 8 \cdot \mu_1 \cdot h^3 \cdot (1 + \bar{\gamma}^2)^{7/2} \cdot \left[M_s + \frac{B}{\mu_p} \cdot (\mu_p - 1)\right]^2} \tag{21}$$

It is assumed that the particles were distributed evenly in one chain. h is the measure of gap between particles in a chain, which is expressed by the ratio of distance between particles and the diameter of particles

$$h = \frac{r_0}{d} \tag{22}$$

For a certain type of MREs, the volume fraction of particles (φ_0) and the properties of particle and elastomer (μ_{p0}, M_{s0}, μ_{10}) are known. Under a specified magnetic field intensity, B_0, the interfacial bond stress of particle chain occurs at the strain for which stress reaches its maximum. Therefore

$$\sigma_y(B) = \max\left\{\sigma_f(\varphi_0, \mu_{p0}, \mu_{10}, M_{s0})\right\}\big|_{B=B_0} \tag{23}$$

With the above microscale modeling, the interface bond strength in the slider process is relevant to the volume fraction and magnetization of magnetic particle, and the relative effective permeability of elastomer to the particles.

Overall, the piece-wise constitutive equations of on-state MRE are derived as follows

$$\begin{cases} \tau + \kappa_r(H) \cdot \dot{\tau} = G_b(H) \cdot (\gamma + \kappa_t(H) \cdot \dot{\gamma}), & |\tau| < \sigma_y(B) \\ \tau + \kappa_r(H) \cdot \dot{\tau} = \eta(H) \cdot \dot{\gamma} + \sigma_y(H) \cdot S\{\dot{\gamma}(t)\}, & |\tau| \geq \sigma_y(B) \end{cases} \tag{24}$$

Theoretical modeling of MRE shock absorbers

According to the MRE model above, a single degree-of-freedom system of MRE shock absorber is established, as shown in Figure 4.

An impact force, $F(t)$, acts on the object with mass, m, which is assumed to be protected. The dynamics equation of this shock absorber system is

$$m \cdot \ddot{x} = -\tau \cdot A + F(t) \tag{25}$$

where τ is the stress of MRE system, and A is the cross section area. In this analysis, the mass of MRE is neglected.

By applying the normal distribution function, Dirac Delta function is used to depict the impact force

$$F(t) = \frac{A_{max}}{\sqrt{\pi}} \cdot e^{-\frac{t^2}{b^2}} \tag{26}$$

where A_{max} is related to the amplitude of impact force, with unit of N, and b is related to the impulse time, with unit of second.

Thus, equation (25) can be rewritten as

$$m \cdot \ddot{x} = -\tau \cdot A + \frac{A_{max}}{\sqrt{\pi}} \cdot e^{-\frac{t^2}{b^2}} \tag{27}$$

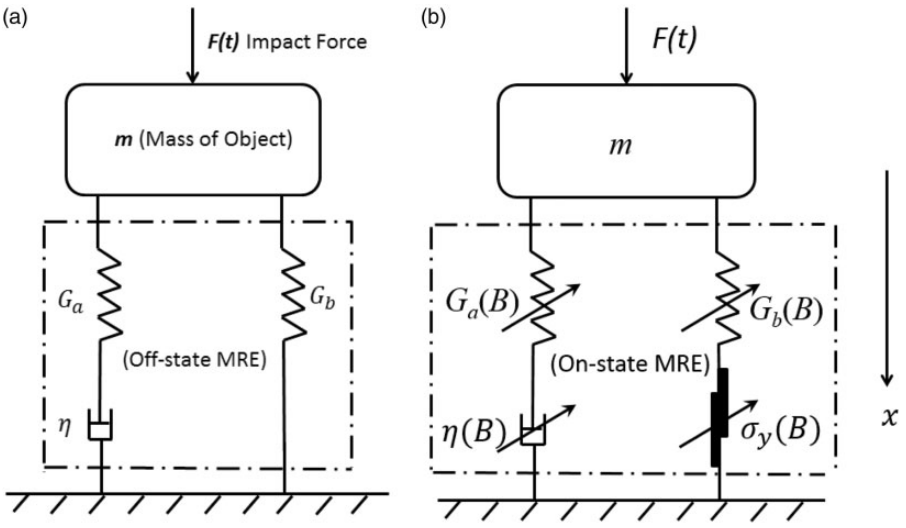

Figure 4. Modeling of MRE shock absorber system. (a) off-state, and (b) on-state.

Substituting the constitutive equations of off-state MRE into the dynamic model, one can obtain

$$\begin{cases} m \cdot \ddot{x} = -\tau \cdot A + \dfrac{A_{max}}{\sqrt{\pi}} \cdot e^{-\frac{t^2}{b^2}} \\ \tau + \kappa_r \cdot \dot{\tau} = G_b \cdot (\gamma + \kappa_t \cdot \dot{\gamma}) \\ \dot{\gamma} = \dfrac{\dot{x}}{L} \end{cases} \tag{28}$$

with the initial conditions

$$x(0) = 0, \quad \dot{x(0)} = 0, \quad \tau(0) = 0 \tag{29}$$

where L is the original size of the system. It is assumed that the object is balanced at the initial position under static loads.

For the on-state MRE, the dynamic equations can be expressed as follows

$$\begin{cases} m \cdot \ddot{x} = -\tau \cdot A + \dfrac{A_{max}}{\sqrt{\pi}} \cdot e^{-\frac{t^2}{b^2}} \\ \begin{cases} \tau + \kappa_r(B) \cdot \dot{\tau} = G_b(B) \cdot (\gamma + \kappa_t(B) \cdot \dot{\gamma}) & |\tau| < \sigma_y \\ \tau + \kappa_r(B) \cdot \dot{\tau} = \eta(B) \cdot \dot{\gamma} + \sigma_y(B) \cdot \tanh\left(\dfrac{\dot{\gamma}}{a}\right) & |\tau| \geq \sigma_y \end{cases} \\ \dot{\gamma} = \dfrac{\dot{x}}{L} \end{cases} \tag{30}$$

The initial conditions are the same as shown in equation (29). In order to analyze the motion of impact system, normalized parameters are introduced as follows

$$\bar{x} = \frac{x}{x_0} \tag{31}$$

$$\bar{t} = \frac{t}{t_0} \tag{32}$$

$$\bar{\tau} = \frac{\tau}{\sigma_s} \tag{33}$$

where x_0, t_0, σ_s are the length, time, and stress constants, respectively. The normalized equation (28) is

$$\begin{cases} \bar{y} = \dot{\bar{x}} \\ \dot{\bar{y}} = -\bar{T} \cdot \bar{\tau} + \bar{Q} \cdot e^{-\bar{N} \cdot (\bar{t})^2} \\ \bar{\tau} + \bar{\eta} \cdot \dot{\bar{\tau}} = \bar{G} \cdot \bar{x} + \bar{K} \cdot \bar{y} \end{cases} \tag{34}$$

with the initial conditions

$$\bar{x}(0) = 0, \quad \dot{\bar{x}}(0) = 0, \quad \bar{\tau}(0) = 0 \tag{35}$$

Similarly, equation (30) can be written as

$$\begin{cases} \bar{y} = \dot{\bar{x}} \\ \dot{\bar{y}} = -\bar{T} \cdot \bar{\tau} + \bar{Q} \cdot e^{-\bar{N} \cdot (\bar{t})^2} \\ \begin{cases} \bar{\tau} + \bar{\eta} \cdot \dot{\bar{\tau}} = \bar{G} \cdot \bar{x} + \bar{K} \cdot \bar{y}, & |\bar{\tau}| < 1 \\ \bar{\tau} + \bar{\eta} \cdot \dot{\bar{\tau}} = \bar{E} \cdot \bar{y} + \tanh\left(\frac{\dot{\bar{y}}}{a}\right), & |\bar{\tau}| \geq 1 \end{cases} \end{cases} \tag{36}$$

with the same initial conditions, as in equation (35), where

$$\bar{T} = \frac{\sigma_s \cdot A}{m \cdot \frac{x_0}{t_0^2}} \tag{37}$$

$$\bar{Q} = \frac{\frac{A_{max}}{\sqrt{\pi}}}{m \cdot \frac{x_0}{t_0^2}} \tag{38}$$

$$\bar{N} = \frac{t_0^2}{b^2} \tag{39}$$

$$\bar{\eta} = \frac{\eta}{G_a \cdot t_0} \tag{40}$$

$$\bar{G} = \frac{G_b}{\sigma_s} \tag{41}$$

$$\bar{K} = \frac{\eta \cdot (G_a + G_b)}{\sigma_s \cdot G_a \cdot t_0} \tag{42}$$

$$\bar{E} = \frac{\eta}{\sigma_s \cdot t_0} \tag{43}$$

Parameters in the theoretical modeling

Parameters identification of MREs

The experimental data in Behrooz et al.[27] are utilized to identify the parameters, G_a, G_b, η, σ_y, in off-state and on-state MREs. The matrix of MRE is the mixture of GE Silicones RTV 615 A and RTV 615 B. The weight fraction of iron particles is 70%. Under a harmonic force input, the synthesized samples are sheared dynamically in zero-magnetic field (off-state) and 0.57 T magnetic field (on-state), respectively.

For the on-state MREs, the interfacial bond strength is calculated first by equations (21) to (23) as 46 kPa. Then, $G_a(B)$, $G_b(B)$, and $\eta(B)$ are estimated by minimizing the error of stress between the model, τ_m, and the experimental data, τ_e. The sum of squared absolute errors, W, is selected as the objective function, which is expressed as

$$W = \sum_{i=1}^{s} (\tau_{mi} - \tau_{ei})^2 \tag{44}$$

where s is the number of the fitting points. The optimization is conducted by using the sequential quadratic algorithm in MATLAB. For the off-state MRE, the parameter G_a, G_b ,and η are estimated by equation (44). The identified parameters are listed in Table 1.

Table 1 shows that both the stiffness and damping at on-state are greater than that at off-state. Hence, the result demonstrates that MRE exhibits variable stiffness capabilities. For example, the stiffness parameter G_a increases more than 60% from about 1.0 MPa at off-state to 1.68 MPa at on-state when the magnetic field is 0.57 T. The dynamic damping increases approximately twice from 0.53 MPa s at off-state to 0.99 MPa s at on-state.

The stress–strain relationships of on-state and off-state MREs are shown in Figure 5. The curves corresponding to E1 and M1 are experimental and model results of on-state MRE, respectively. And, E2 and M2 denote the results of off-state MRE. It presents an obvious phase angle between stress and strain. At off-state, the stress–strain curve exhibits fusiform loops. At on-state, there is a relative expansion on the ends of the loops, which is due to the magnetic field-induced interface bond strength, $\sigma_y(B)$. When the excited stress is greater than $\sigma_y(B)$, the particles slide along the interface between them and matrix. As mentioned in equation (21), the bond strength is determined by the volume fraction of particles, φ, and saturated magnetization of magnetic particle, Ms. As φ and Ms increase, the bond strength enhances. The area enclosed by the stress–strain curve represents the energy dissipations within one impact cycle, which expands at on-state than off-state due to the effect of external magnetic field. The slope angle of the loop means the stiffness of MREs, which increases in the magnetic field. The comparisons between the experimental results and the theoretical predictions demonstrate that the modified multiparameter models can predict MRE's performances.

Liu et al.[28] shows, when the strain rate is less than 0.09 s^{-1}, the loading has little effect on the mechanical behaviors of rubber material. Hence, the strain rate of MREs is neglected in the present work.

Table 1. Parameters in theoretical model.

Flux density (T)	G_a (MPa)	G_b (MPa)	η (MPa s)	σ_y (k Pa)
0	1.01	0.88	0.53	–
0.57	1.68	1.07	0.99	46

Parameters for MRE shock absorbers

The parameters in impulse function are $A_{max} =$ 25,000 N, and $b = 1/1000$ s. Hence, the force amplitude is 1.4×10^4 N, and the lasting time of the impact

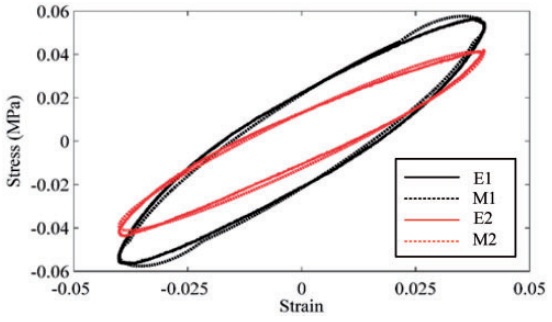

Figure 5. The stress–strain relationship of MREs (E: experimental results, M: model results, 1: on-state, 2: off-state).

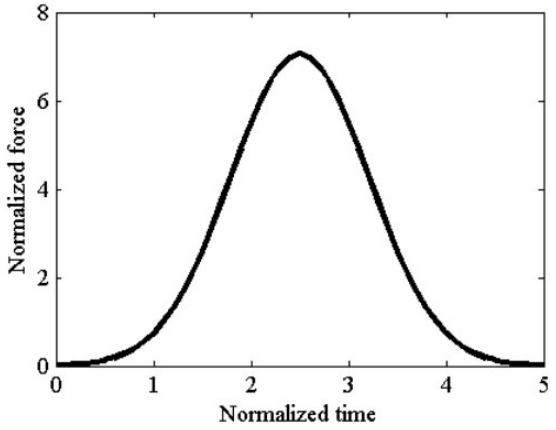

Figure 6. The impulse force function.

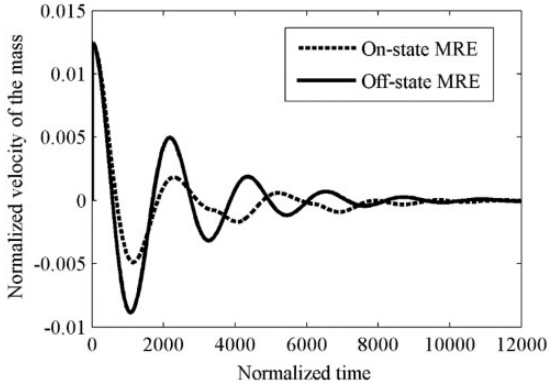

Figure 7. Velocity responses of the protected object in MRE system.

function is 5×10^{-3} s. The normalized impulse force versus normalized time is shown in Figure 6.

The mass of the object, m, is 20 kg. The cross section area is 10 cm^2. The original size, L, is 1 cm. Also, the normalized length, time, and stress constants are $x_0 = 0.1$ m, $t_0 = 10^{-3}$ s, and $\sigma_s = 46$ kPa, respectively.

According to the parameters in MRE model and impact system above, the dynamic equations of MRE-based shock absorber, equations (34) and (36), could be solved numerically. The dynamic responses of MRE shock absorbers at off-state and on-state are discussed below.

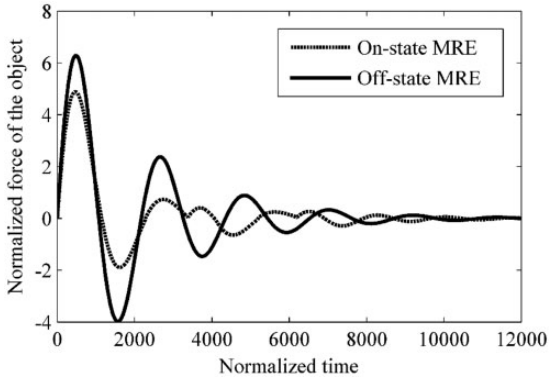

Figure 8. Comparison of force responses of the protected object in MRE system.

Results and discussions

Velocity responses and residual kinematic energy

Most residual energy of the shock absorber system could be expressed by the kinematic energy of the protected mass, which is proportional to the square of its velocity if the mass is a constant. The less kinetic energy of the object is, the more energy is dissipated by the MRE shock absorbers. Figure 7 shows the normalized velocity–time responses of the protected object, which reaches the peak (0.013) immediately (at normalized moment 4.46) after the impulse input. Then, it experiences several oscillations until stable at balance. It is also found that the velocity amplitude at on-state is attenuated quicker than that at off-state. Therefore, MRE under a given magnetic field can dissipate more energy than the off-state one.

Force responses

The impact force peak on the protected object is an important index to evaluate the energy dissipation capability of the energy absorbers. The comparison of the normalized impact force on the protected object between off- and on-state MRE systems is shown in Figure 8.

In Figure 8, the first peak force in the on-state MRE system reduces approximately 30% in the positive direction as compared with the off-state system, from 4.82 to 6.21. The second peak force in the on-state MRE reduces more than 50% in the negative direction as compared with the off-state one, from 3.98 to 1.83. This demonstrates that the force acting on the object can be greatly reduced by the MREs under an applied magnetic field, compared with the off-state one. This prediction result is in agreement with the experimental results.[14] This phenomenon is attributed to the field-induced stress of on-state MREs. Without the applied magnetic field, the stress of MRE keeps increasing until it reaches the maximum deformation. However, under an applied magnetic field, the friction element plays a major role in dissipating energy. This element functions similar to a ''valve.'' When the stress exceeds the field-induced strength, the friction element begins to slip, and the overall stress of MRE instantly reduces.

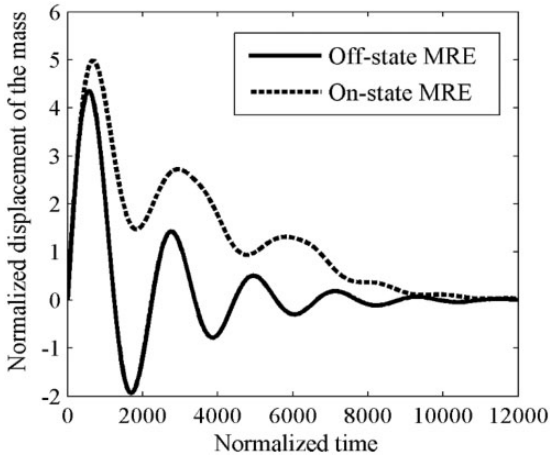

Figure 9. Normalized displacement responses of the protected object.

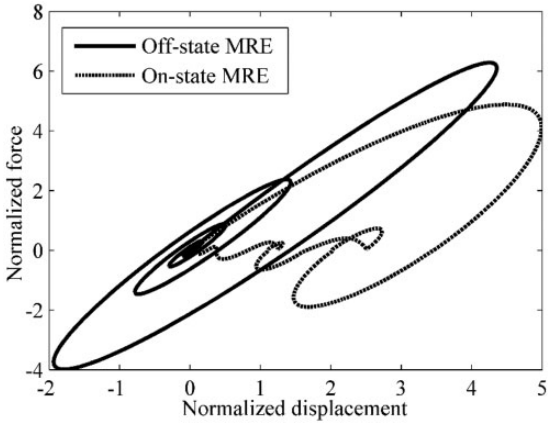

Figure 10. Force–displacement curves of the protected object in the MRE system.

Therefore, MREs at on-state can attenuate peak force on the protected object more than MREs at off-state.

Displacement responses

Dynamic displacement of protected object is the calculation base of transient velocity and acceleration, which determines the installation space of absorbers. Comparisons between off- and on-state MREs for the normalized displacement history of the protected object are shown in Figure 9.

In Figure 9, it can be seen that the maximum displacement of the object in the on-state MRE shock absorber is greater than that in the off-state one. Also, the displacement in on-state MRE system is always positive. This is due to the "locking" effect of the nonlinear friction element in the modeling of on-state MRE which moves only when the overall stress of MRE is greater than the field-induced strength. When the stress is less than the strength, the friction element locks and the displacement is only recorded. However, the displacement of the object in off-state MRE system is either positive or negative. It is because that the deformation of dashpot and springs in the modeling of off-state MRE is reversible.

Force–displacement curve and energy dissipation

Figure 10 shows the force–displacement curves of the protected object in the off- and on-state MRE system.

It is assumed that the total energy which is determined by the impulse force is conserved. The enclosed area of the curve in Figure 10 denotes the energy loaded on the object. Hence, the less the enclosed area is, the more energy is dissipated by the MRE system. As shown in Figure 10, we can calculate that the normalized energy loaded on the protected object in the off-state and on-state MRE system are 379.1 and 357.5, respectively. It demonstrates that the MRE-based shock absorber in the on-state can dissipate more energy. This conclusion agrees with that from Figure 7.

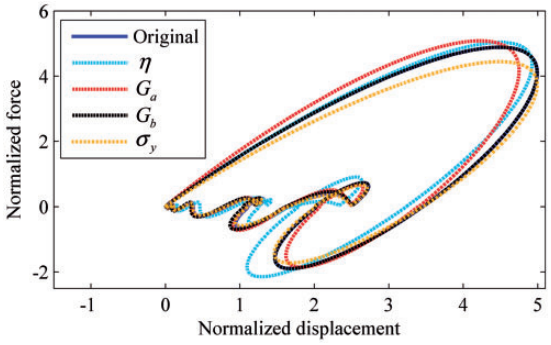

Figure 11. The sensitivity of parameters on the force–displacement curve.

Sensitivity of influence factors on energy dissipation

For the on-state MRE system, we investigate the sensitivity of key parameters, such as G_a, G_b, η, and σ_y on the dynamic responses of the object. Let only one studied variable increases by 10% while the others are fixed. The comparisons of dynamic responses are shown in Figures 11 to 13. The peak force with different parameters is listed in Table 2.

As shown in Figures 11 to 13, the stiffness G_a changes the slope of the displacement–force curve. The increment of G_a increases the peak force, while reduces the maximum displacement. However, the

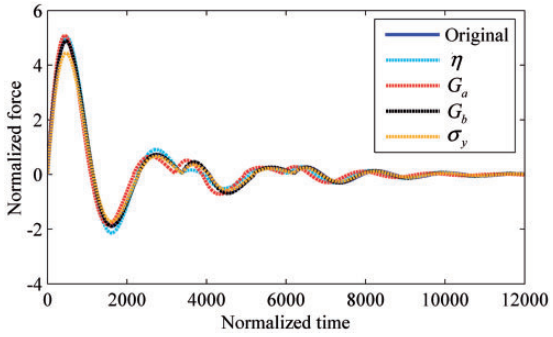

Figure 12. The sensitivity of parameters on the force–time curve.

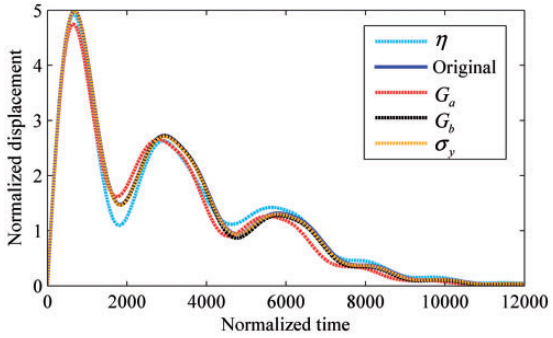

Figure 13. The sensitivity of parameters on the displacement–time curve.

Table 2. The sensitivity of parameters on the dynamic responses.

	Original	G_a (10%↑)	G_b (10%↑)	η (10%↑)	σ_y (10%↑)
The peak force	4.88	5.08 (4.1%↑)	4.88 (0%)	5.06 (3.6%↑)	4.44 (9.1%↓)

spring with stiffness G_b has little effect on the dynamic responses of the object. It is because that, in the on-state MRE, the spring with stiffness G_b works with the friction element. Once the friction element slips, the length of this spring keeps unchangeable. Hence, the friction component dominates the dynamic behavior of MRE more remarkably, compared with the spring with stiffness G_b. Additionally, the damping parameter, η, influences the vibration process of the protected object. The increment of η slightly enhances the peak force, while largely decreases the displacement amplitude in the first valley. It is worth mentioning that the increment of the field-induced stress reduces the peak force loaded on the object, as shown in Table 2. We also found in Figure 11 that the enclosed area of displacement–force shrinks with σ_y increasing, which demonstrates that the increment of field-induced stress enhances the energy dissipation capacity of MREs. From the above microscale model, it is found that σ_y is proportional to the volume fraction of magnetic particles. Therefore, in the application of MREs for shock resistance, the field-induced stress at a greater value is expected, which can be achieved by the increment of volume fraction of particles and the decrement of the relative permeability of elastomer matrix as shown in equation (21). This guideline may direct the design and manufacture of MRE specimen with high energy dissipation capacity.

Conclusions

The modified multiparameter models are proposed to depict the mechanical performances of MREs, and their constitutive equations at off-state and on-state are derived, respectively. All parameters in MRE model are identified based on the published experimental data.

The theoretical models of MRE-based shock absorber are established and the dynamic impact responses are solved. A comparative study between off-state and on-state MRE shock absorber shows that, on-state MRE can dissipate more impact energy and attenuate peak force on the protected object faster than the off-state one.

It is also found that the energy dissipation mechanisms come mainly from the interfacial friction between particles and matrix, and the increase on stiffness and dynamic viscosity of the rubber matrix provide reverse contribution on the shock mitigation, while the interfacial bond stiffness has little influence on the dynamic responses.

To improve the energy dissipation capability, the field-induced stress at a greater value is suggested for the design of MRE-based shock absorber. This study shows that MREs are potential candidates in the application of adaptive shock mitigation.

Declaration of Conflicting Interests

The author(s) declared no potential conflicts of interest with respect to the research, authorship, and/or publication of this article.

Funding

The author(s) disclosed receipt of the following financial support for the research, authorship, and/or publication of this article: The authors would like to express their gratitude for the support of the National Natural Science Foundation of China (No.51175485), China Postdoctoral Science Foundation (No. 2015M582141), Innovation Postdoctoral Science Foundation of Shandong Province (No. 201503014).

References

1. Andrzej M and Mikolaj H. Application of magnetorheological fluid in industrial shock absorbers. *Mech Syst Signal Pr* 2012; 28: 528–10.
2. Ahmadian M and Norris JA. Experimental analysis of magnetorheological dampers when subjected to impact and shock loading. *Commun Nonlinear Sci* 2008; 13: 1978–1985.
3. Dong XM. Semi-active control of magnetorheological variable stiffness and damping seat suspension with human-body model. *Int J Vehicle Des* 2013; 63: 119–136.
4. Browne AL, Mccleary JD, Namuduri CS, et al. Impact performance of magnetorheological fluids. *J Intell Mater Syst Struct* 2009; 20: 723–728.
5. Gong X, Zhang X and Zhang P. Fabrication and characterization of isotropic magnetorheological elastomers. *Polym Test* 2005; 24: 669–676.
6. Watson JR. Method and apparatus for varying the stiffness of a suspension bushing. Patent 609,353, USA, 1997, No. 5.
7. Kallio M. *The elastic and damping properties of magnetorheological elastomers*. Finland: Espoo, VTT Publications, 2005.
8. Li W, Zhou Y and Tian T. Viscoelastic properties of MR elastomers under harmonic loading. *Rheol Acta* 2010; 49: 733–740.
9. Li Y, Li J, Li W, et al. A state-of-the-art review on magnetorheological elastomer devices. *Smart Mater Struct* 2014; 23: 123001(1–24).
10. Ginder JM, Clark SM, Schlotter WF, et al. Magnetostrictive phenomena in magnetorheological elastomers. *Int J Mod Phys B* 2002; 16: 2412–2418.
11. Yeh Z and Shih Y. Dynamic characteristics and dynamic instability of magnetorheological material based adaptive beams. *J Compos Mater* 2006; 40: 1333–1359.
12. Chokkalingam R, Pandi RS and Mahendran M. Magnetomechanical behavior of Fe/PU magnetorheological elastomers. *J Compos Mater* 2011; 45: 1545–1552.
13. Sun L, Li W, Guo S, et al. A magnetorheological-elastomer-based energy absorption device (MREBEAD) for car crash protection. *Int J Vehicle Des* 2013; 63: 223–240.
14. Fu J, Yu M, Dong XM, et al. Magnetorheological elastomer and its application on impact buffer. *J Phys Conf Ser* 2013; 412: 012032(1–10).
15. Leng D, Sun L, Gordaninejad F, et al. The dynamic performance of magnetic-sensitive elastomers under impact loading. *Smart Mater Struct* 2015; 24: 045023.
16. Norouzi M, Alehashem SMS, Vatandoost H, et al. A new approach for modeling of magnetorheological elastomers. *J Intell Mater Syst Struct*, Epub ahead of print 2015. DOI: 10.1177/1045389X15615966).
17. Danas K, Kankanala SV and Triantafyllidis N. Experiments and modeling of iron-particle-filled magnetorheological elastomers. *J Mech Phys Solids* 2012; 60: 120–138.
18. Galipeau E and Castañeda PP. A finite-strain constitutive model for magnetorheological elastomers: magnetic torques and fiber rotations. *J Mech Phys Solids* 2013; 61: 1065–1090.
19. Davis LC. Model of magnetorheological elastomers. *J Appl Phys* 1999; 85: 3348.
20. Kankanala SV and Triantafyllidis N. On finitely strained magnetorheological elastomers. *J Mech Phys Solids* 2004; 52: 2869–2908.
21. Eem S, Jung H and Koo J. Modeling of magnetorheological elastomers for harmonic shear deformation. *IEEE Trans Magnetics* 2012; 48: 3080–3083.
22. Li Y, Li J, Tian T, et al. A highly adjustable magnetorheological elastomer base isolator for applications of real-time adaptive control. *Smart Mater Struct* 2013; 22: 095020.
23. Yang J, Du H, Li W, et al. Experimental study and modeling of a novel magnetorheological elastomers isolator. *Smart Mater Struct* 2013; 22: 117001.
24. Chen L and Jerrams S. A rheological model of the dynamic behavior of magnetorheological elastomers. *J Appl Phys* 2011; 110: 013513(1–6).
25. Wang X and Gordaninejad F. A new magnetorheological fluid-elastomer mount: phenomenological modeling and experimental study. *Smart Mater Struct* 2009; 18: 095045(1–9).
26. Jolly MR, Carlson JD and Munoz BC. A model of the behavior of magnetorheological materials. *Smart Mater Struct* 1996; 5: 607–614.
27. Behrooz M, Wang X and Gordaninejad F. Modeling of a new magnetorheological elastomer-based isolator. In: *SPIE Proc*, vol. 8688, 2013, p. 86880Z.
28. Liu ZR, Tang HY, Zheng YL, et al. *The industry manual of rubber materials*. Beijing: Chemical Industry Press, China, 1992.